MATERIALE PLASTICE
https://revmaterialeplastice.ro
https://doi.org/10.37358/Mat.Plast.1964

Effect of Phenolic Resin Coating Thickness on Mechanical Properties and Corrosion Resistance of Metal Materials

DIYAO ZHANG, LEI YUAN, JINGKUN YU*
School of Metallurgy, Northeastern University, Shenyang, 110819, P. R. China

***Abstract**: In the realm of petrochemical and other industries, metal materials face threats such as impact and high-temperature electrochemical corrosion. Consequently, there has been significant attention towards organic coatings that effectively attenuate impact forces while simultaneously providing a barrier against corrosive agents. The thermosetting phenolic resin 2130, known for the facile curing process, exceptional thermal stability, water resistance, corrosion resistance, and superior mechanical properties post-curing, finds extensive applications in the field of coatings. To address the challenge of depositing a complete and uniform resin coating on complex workpieces, coatings with varying thicknesses on the surface of 304 stainless steel were deposited via rotary evaporation combined with long-term low-temperature drying. The relationship between coating thickness and mechanical properties, as well as corrosion resistance, was investigated and analyzed through a comprehensive approach involving mechanical testing, electrochemical analysis, and long-term service weight loss assessment. The results demonstrated that the coatings deposited on the metal surface exhibited excellent integrity and compactness. Moreover, an increase in coating thickness led to a significant reduction in material corrosion rate. The coatings exhibited excellent substrate adhesion and flexibility, thereby providing effective protection against impact on the metal substrate. The relationship between the thickness of the coating and the surface roughness was evident, while the flexibility of the coating first increased and then decreased with the increase of coating thickness. When the coating thickness was 7 μm, the maximum surface roughness of the coating measured 0.44 μm. Under these conditions, the impact toughness of the coating reached the peak, exhibiting a ductile fracture mode and showcasing superior comprehensive mechanical properties. The findings of this study will offer theoretical support for the investigation and formulation of resin coatings in subsequent industrial production.*

***Keywords:** phenolic resin, rotary evaporation, coating thickness, corrosion resistance, mechanical property*

1. Introduction

The utilization of metal materials is frequently observed in diverse challenging industrial environments [1, 2]. Therefore, metal materials are exposed to various failure threats, encompassing physical failures such as external impact damage, and chemical failures primarily manifested as electrochemical corrosion [3, 4]. While improving the properties of the material itself, the preparation of protective coatings has also attracted much attention. Although the traditional corrosion-resistant hard coating provides effective physical protection after deposition, the presence of a conductive metal coating defect or damage can lead to the attachment of corrosive medium to exposed substrate areas. This creates an electric potential difference between the coating and substrate, resulting in the formation of a galvanic battery system in the solution that accelerates electrochemical corrosion [5, 6]. As material service temperature gradually increases, the rate of electrochemical corrosion significantly escalates. The consideration of finding a coating that is better suited for the current environment is imperative. The organic coating exhibits robust water resistance, exceptional corrosion resistance, and a high adhesive strength between the metal matrix and the hard coating, while also possessing a certain degree of flexibility [7-9]. Currently, the application of highly elastic resin coatings on metal surfaces represents

**email: yujk@smm.neu.edu.cn*

a remarkably effective approach to prevent both impact failure and corrosion in metals. Moreover, the utilization of resin coatings can significantly extend the service life of steel by more than several times [10].

When selecting organic coatings, epoxy resin and phenolic resin are the most frequently utilized options [11-13]. Both materials possess the same advantageous characteristic, namely their exceptional physical isolation performance, enabling the formation of a compact film on the metal matrix surface. This film effectively shields against corrosive substances such as water vapor and reduces direct contact between the metal matrix and the surrounding corrosive environment [14, 15]. In contrast to the intricate curing conditions of epoxy resin, phenolic resin exhibits rapid heat-curing capabilities within the temperature range of 170~200^{o}C, it also can be slowly cured at ambient or slightly elevated temperatures while retaining excellent high-temperature resistance post-curing [16]. The phenolic resin coating is frequently applied to the external walls of boilers, oil and gas pipelines, and other high-temperature environments in practical production due to this characteristic. Through prolonged baking, the coating gradually solidifies into a film, effectively isolating corrosive mediums and alleviating the external impact, on the base material thereby providing effective protection. In the context of electrochemical corrosion protection, the extent of material corrosion is determined by the magnitude of current passing through it, with higher levels of corrosion resistance observed at lower internal currents within the material [17]. The phenolic resin exhibits robust dielectric properties and high internal resistance. Upon application as a coating on the metal substrate surface, it induces a significant increase in surface resistance, effectively mitigating the extent of electrochemical corrosion [18-20].

In recent years, the majority of research in phenolic resin coating has been focused on incorporating modified resins and filler additives to enhance the properties of the coating. However, the curing process of resin is highly intricate, and most studies solely concentrate on enhancing coating properties at a specific thickness without considering whether variations in resin coating thickness would impact the post-curing coating properties. The thermosetting phenolic resin 2130 was employed as the film-forming material in this study, while a rotary evaporation method was devised to address the challenge of achieving complete and uniform flexible resin coating on complex structural surfaces using conventional processes. Consequently, a dense phenolic resin coating with varying thicknesses was successfully fabricated on metal substrates. The present study examined the correlation between coating thickness on the substrate surface and the corrosion resistance as well as mechanical properties.

2. Materials and methods

2.1. Materials

In this study, the thermosetting phenolic resin 2130 (Borun Refractory Materials Company, China) was the raw material for the coating whose molecular structure and properties are shown in Figure 1 and Table 1. Ethanol (C_2H_6O, Sinopharm Chemical Reagent Co. Ltd., China, 99.7 %) was used as the solvent of phenolic resin. The metal material was 304 stainless steel (Xinghui Metal, China). Acetone (C_3H_6O, Sinopharm Chemical Reagent Co. Ltd., China, 99.7 %) was utilized as a metal surface degreasing agent for the pretreatment of metal materials, while deionized water (H_2O, Sinopharm Chemical Reagent Co. Ltd., China) was employed to remove any debris from the metal surface.

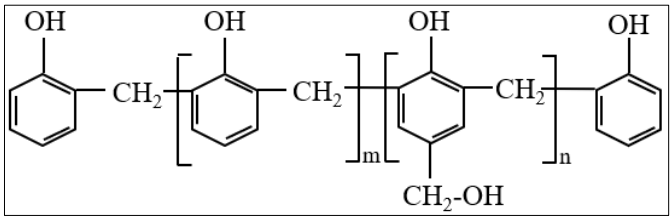

Figure 1. Phenolic resin 2130 structural formula

Table 1. Properties of phenolic resin 2130

Model	Solid content	moisture	free phenol	Viscosity(cp/25℃)
Phenolic resin 2130	≥70	≤4	7-10	2000-3000

2.2. Coating process

A rotary evaporator (RE-52AA, Yarong, China) was used to deposit the phenolic resin coating on the surface of the metal matrix. Prior to the coating preparation, the metal surface underwent a meticulous sanding process ranging from 400 # to 800 # using sandpaper, followed by degreasing, ultrasonic cleaning, and subsequent drying. The phenolic resin solution was prepared using 90 vol% ethanol as the solvent and 10 vol% of thermosetting phenolic resin 2130 as the solute. The samples in the solution were preheated in a rotary evaporator at 60°C with 100 rpm for 10 min, followed by subsequent heating at 90°C for durations of 10, 20, and 30 min respectively. The coating was cured at 60°C for 24 h in an oven (WHL-25AB, Taisite, China), resulting in the formation of phenolic resin dry films with varying thicknesses. The detailed coating preparation process is illustrated in Figure 2, while Table 2 presents the samples prepared using various process parameters. The surface and interface of the coatings were observed by a field emission scanning electron microscope (SEM, JSM-7800F, JEOL, Japan).

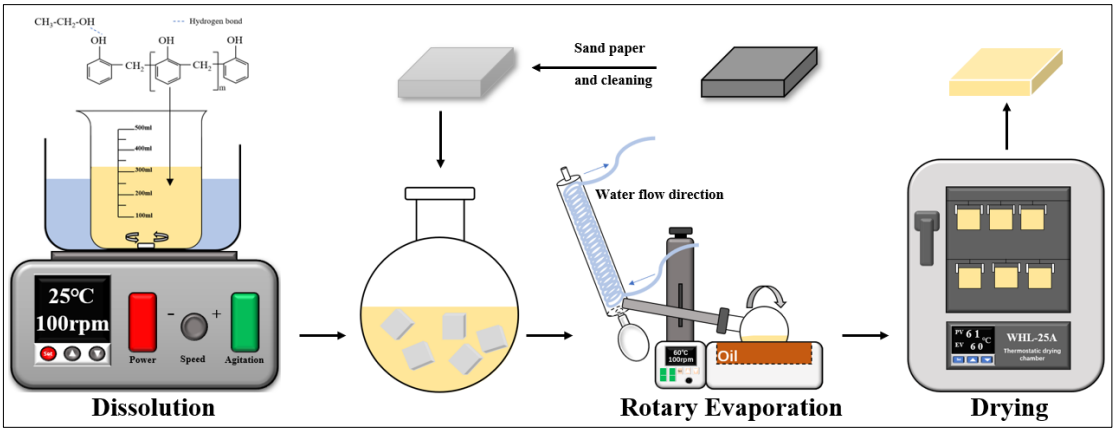

Figure 2. Coating preparation process

Table 2. Coating number corresponding process

Sample	Processing mode
Coating 0	Original 304 stainless steel
Coating 1	(60 ℃,100 rpm,10 min) + (90℃,100 rpm, 10 min)
Coating 2	(60 ℃,100 rpm,10 min) + (90℃,100 rpm, 20 min)
Coating 3	(60 ℃,100 rpm,10 min) + (90℃,100 rpm, 30 min)

2.3. Mechanical property measurement

The mechanical properties test of the phenolic resin coating was conducted to evaluate the flexibility, impact resistance, and adhesion. The test methods refer to GB/T 1731-93, GB/T 1732-1993, and GB/T 9286-1998 respectively. In the flexibility test, the 304 stainless steel sheet coated with a protective layer underwent a 180° bend around shaft rods of varying diameters. After subjecting the coating to ten repeated bending cycles, the presence of fracture burrs along the edges was examined, and the minimum diameter of the shaft rod with intact coating was adopted as a metric for assessing the flexibility of the coating. During the impact resistance test, the coated sheet was positioned beneath the paint film impactor, and the hammer was elevated to varying heights in order to impart force onto the metal. The impact resistance of the coating was assessed by examining the extent of damage to both the coating and the substrate. In the adhesion test, 100 grids were drawn horizontally and vertically on the surface of the

coating at intervals of 1 mm. After applying the tape, it was repeatedly torn off ten times and the integrity of the coating at the grid edge was observed to assess its adhesion.

2.4. Corrosion resistance test

The corrosion resistance of the coating was evaluated using an electrochemical workstation (CS350H, Corrtest, China), with 3.5% NaCl solution as the corrosive medium. The three-electrode cell consisted of a saturated calomel reference electrode (SCE) filled with saturated KCl solution, serving as the reference electrode (RE), a platinum auxiliary electrode with an exposed surface area of 10×10 mm^2 acting as the counter electrode (CE), and the sample with an exposed surface area of 0.5 cm^2 functioning as the working electrode (WE). To minimize error interference, the sample was immersed in a 3.5% NaCl solution for 20 min prior to the electrochemical test. Subsequently, the open circuit potential was maintained at 300s until reaching a stable potential. The frequency range for the electrochemical impedance test was set from 0.01 Hz to 10^5 Hz, and a sinusoidal perturbation signal with an amplitude of 10 mV was applied. The obtained test results were subsequently fitted using ZsimpWin. The high and low potentials of the potentiodynamic polarization curve were ±0.5 V relative to the open circuit potential while maintaining a scanning rate of 5 mV/s. Considering the diverse service environments, following GB/T 7901-1999, wet air hanging specimens were established at a temperature of 30°C and humidity of 80%, while soaking hanging specimens in a 3.5% NaCl solution. The weighing analysis was conducted at intervals of 100 h, while the formation of surface corrosion products was observed through electron microscopy.

3. Results and discussions

3.1. Curing of the coating and bonding with metal matrix

The bonding mechanism between phenolic resin and metal matrix is commonly regarded as a combination of adsorption theory and mechanical interlocking theory. The hydroxyl group (-OH), which is a polar functional group in the elongated molecular chain of the resin, establishes a hydrogen bond with the hydroxyl group present on the oxide film of the metal surface. Simultaneously, upon curing, the resin solution establishes a mechanical interlocking structure within defects such as pits and cracks that penetrate the metal surface, thereby securely affixing the resin coating onto the metal matrix. The successful curing process, based on the aforementioned theories, necessitates the exceptional wettability of the resin solution with the metal matrix. Ethanol stands out as one of the most extensively employed organic solvents. The mixed alcohol-phenolic resin solution exhibited excellent metal matrix wetting properties.

The phenolic resin attached to the metal surface and the curing reaction occurred during the drying process. The thermal curing reaction of the phenolic resin is highly intricate, with multiple concurrent curing reactions taking place. The condensation reaction between the active hydrogen on the ortho position of the benzene ring and the hydroxymethyl group in the long molecular chain of phenolic resin is exemplified in Figure 3, illustrating the process of intermolecular crosslinking and curing to form a three-dimensional network structure.

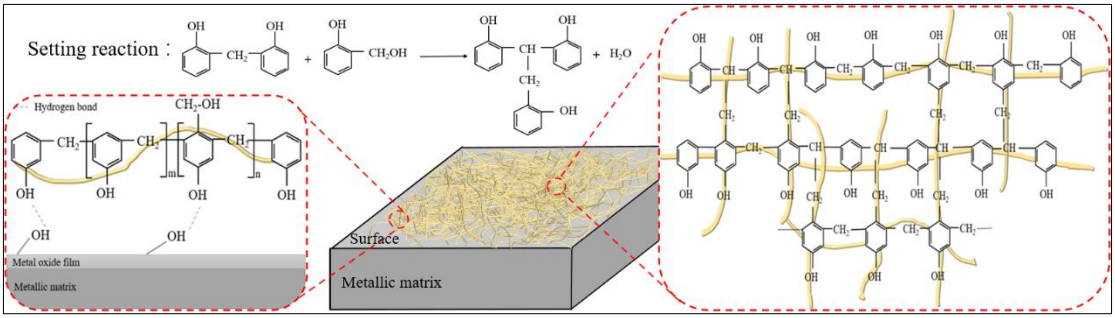

Figure 3. The curing mechanism and structure of phenolic resin coating on metal surface

Figure 4 shows the cross-sectional and surface morphology of the coating after curing. It can be found that the rotary evaporation method combined with the low-temperature drying process yielded phenolic resin coatings of varying thicknesses, which formed a stable and compact film on the metal matrix surface. The corresponding coating thickness and surface roughness data are presented in Table 3.

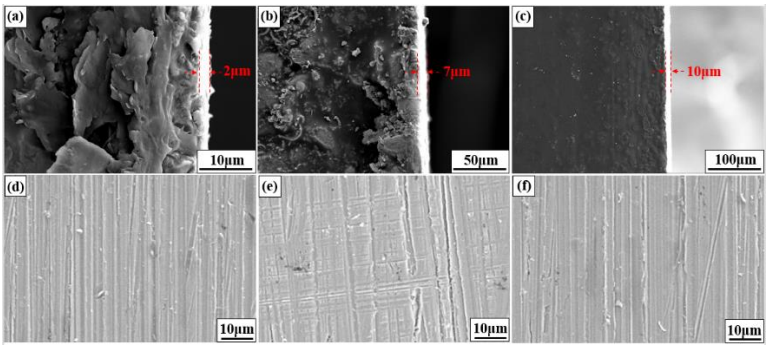

Figure 4. SEM images of the cross-section and surface morphology of each coating:(a), (d) Coating 1; (b), (e) Coating 2; (c), (f) Coating 3

Table 3. Thickness and surface roughness of each coating.

Sample	Coating thickness	Surface roughness (*Ra*)
Coating 1	2 μm	0.22 μm
Coating 2	7 μm	0.44 μm
Coating 3	10 μm	0.28 μm

3.2. Analysis of mechanical properties of coatings

3.2.1. Adhesion of coatings

According to the National Standard GB/T9286-1998, a total of 100 grids were meticulously drawn both horizontally and vertically on the coated samples at precise intervals of 1 mm. Subsequently, an adhesive tape was meticulously affixed onto the coating surface and then delicately removed at the minimum possible angle. After undergoing ten repetitions of this process, it can be observed in Figure 5b, d, f that the incision edges of coatings 1, 2, and 3 remained smooth and did not exhibit any signs of detachment after the ten tests. The adhesion between the coatings and the metal matrix was found to be excellent. As indicated in Table 4, all coatings exhibited a superior level of adhesion [21, 22].

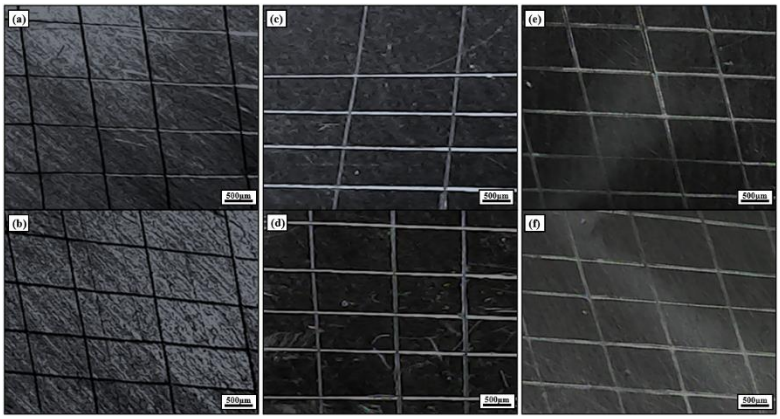

Figure 5. Hundred grid test of each coating: (a), (b) Coating 1 test once, test ten times; (c), (d) Coating 2 test once, ten times; €, (f) Coating 3 test once, test ten times

Table 4. Hundred grid test grade of each coating.

Sample	ISO Level	ASTM Level
Coating 1	0	5B
Coating 2	0	5B
Coating 3	0	5B

3.2.2. Impact resistance of coatings

As depicted in Figure 3, the phenolic resin undergoes a curing process to form a well-defined three-dimensional network structure. The molecular chains are intricately intertwined with each other, resulting in the coating possessing excellent impact resistance and flexibility [23, 24]. The three-dimensional network dispersed the impact force upon the metal matrix surface, thereby preventing stress concentration at a single location and effectively safeguarding the integrity of the metal matrix. The 304 stainless steel (50×20×0.3 mm^3) was coated with phenolic resin and the impact resistance of the coating was tested by the paint film impactor. In the experimental results, the value (kg·cm) obtained by multiplying the weight of the hammer (0.1kg) and the drop height (cm) was used as the index to evaluate the impact resistance. The state of the metal surface is shown in Figure 6, and the specific data is recorded in Table 5.

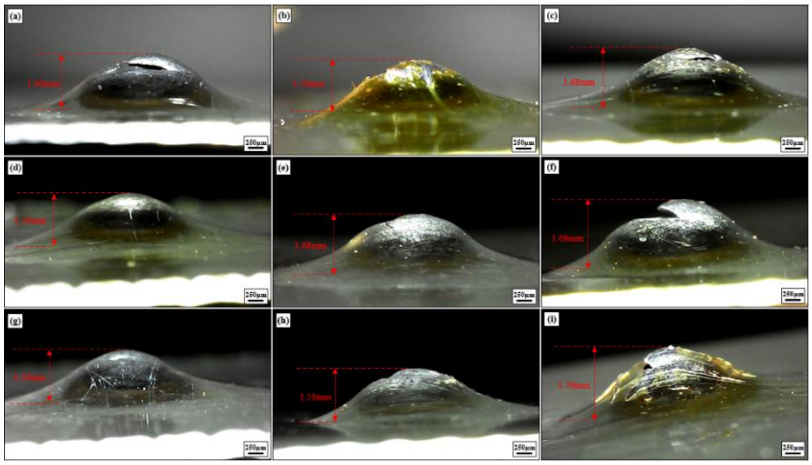

Figure 6. Impact test of each coating at different heights: (a) Coating 0/70 cm; (b), (c) Coating 1/70 cm, 75 cm; (d), (e), (f) Coating 2/70 cm, 75 cm, 80 cm; (g), (h), (i) Coating 3/70 cm, 75 cm, 80 cm

Table 5. The matrix condition and impact pit depth of each coating after impact at different heights

Sample	70 cm	75 cm	80 cm
Coating 0	Rupture 1.60 mm	/	/
Coating 1	Crack 1.65 mm	Rupture 1.68 mm	/
Coating 2	Health 1.56 mm	Crack 1.62 mm	Rupture 1.80 mm
Coating3	Health 1.56 mm	Health 1.58 mm	Rupture 1.76 mm

During the descent of the heavy hammer, gravitational potential energy was transformed into kinetic energy, which impacted the metal surface with force. The results presented in Table 5 demonstrate a positive correlation between the increase in coating thickness and the corresponding increase in the critical height required for fracture initiation of the metal matrix by heavy hammer impact. The metal matrix was capable of absorbing a greater amount of impact kinetic energy when shielded by the protective coating. Taking the hammer height of 70 cm as an example, the depth of the impact pit on the

metal surface gradually decreased from 1.68 mm to 1.58 mm with increasing coating thickness. When the coating thickness increased from 2 μm to 7 μm, the impact resistance index of the uncoated matrix increased from 7 kg·cm to 8 kg·cm. However, further increasing the coating thickness did not result in any additional improvement in the impact resistance of the steel plate.

3.2.3. Flexibility of coatings

Phenolic resin coatings with different thicknesses were prepared on the 304 stainless steel sheets (50×10×0.3 mm^3) and tested one by one for shaft rods with diameters from 10 mm to 1 mm according to the National Standard GB/T 1731-93. The phenolic resin coatings exhibited complete integrity after undergoing a 180° bending test with the minimum shaft rod diameter (1 mm) as demonstrated in Table 6, without any cracks. On this basis, repeat the bending operation ten times. The coatings exhibit a smooth and intact surface without any cracks or damages, as depicted in Figure 7.

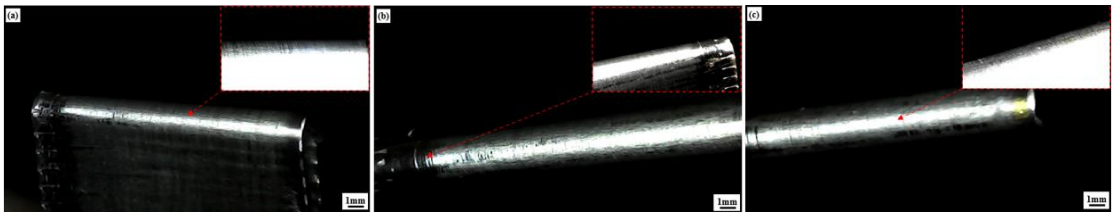

Figure 7. Ten bending tests of the minimum rod diameter of each coating: (a) Coating 1; (b) Coating 2; (c) Coating 3

Table 6. The minimum bending rod diameter and coating state of each coating

Sample	Minimum rod diameter	One test coating state	Ten tests of coating state
Coating 1	1 mm	Health	Health
Coating 2	1 mm	Health	Health
Coating 3	1 mm	Health	Health

Although the increase in coating thickness provided a protective function for the metal, it can be observed from Figure 8a, h that when the metal matrix of coatings 1 and 3 experiences breakdown, brittle fracture occurs within the coatings, causing detachment of surrounding coating layers from the matrix [25]. The impact height was gradually increased from 70 cm to 85 cm. It was observed that irrespective of the presence or absence of metal matrix fracture, coating 2 exhibited a strong bond with the metal matrix, and no signs of burrs or coating fragments were detected around the fractured metal. Furthermore, the bonding between the fractured coating and the metal matrix remained intact, indicating a ductile fracture mode for coating 2.

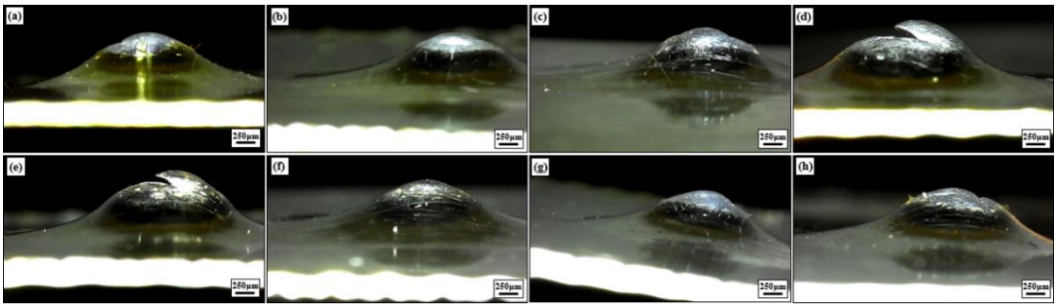

Figure 8. The state of each coating after impact at different heights: (a) Coating 1/70 cm; (b), (c), (d), (e) Coating 2/70 cm, 75 cm, 80 cm, 85 cm; (f), (g), (h) Coating 3/70 cm, 75 cm, 80 cm

The curing shrinkage time of phenolic resin coatings varies with their thickness. The changes in curing shrinkage volume of phenolic resin form the depth of grooves, which was manifested in the roughness of each coating surface. The fracture of the coating was attributed to stress concentration,

with stress typically exhibiting higher levels of concentration in the bulge and groove regions. As depicted in Figure 9, when the metal surface coating is subjected to an impact force, the smoothness of the coating disperses and distributes the impact force uniformly in all directions. When the surface roughness of the coating increased, the surface groove deepened. When subjected to the same impact, a stress concentration area formed at the deep groove of the coating surface, thereby increasing the likelihood of fracture occurrence. The majority of the impact force will be distributed along the deep groove of the coating surface. When the coating was breached, under shear force, failure of the coating manifests as tearing along the deep groove direction without collapse of either side. The states of each coating at different impact heights are documented in Table 7.

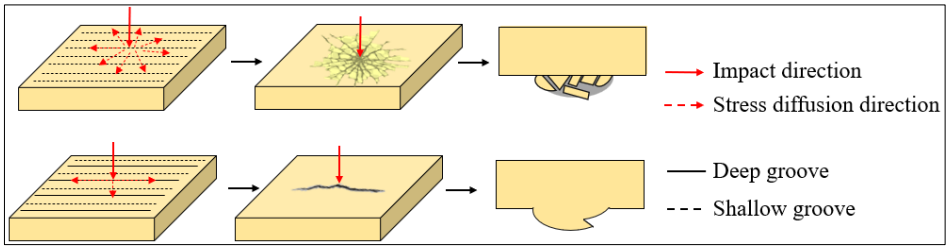

Figure 9. Coating fracture mechanism under different roughness

Table 7. The states of each coating after impact at different heights.

Coating state	70 cm	75 cm	80 cm	85 cm
Coating 1	Rupture	/	/	/
Coating 2	Health	Smooth edge without burrs	Smooth edge without burrs	Smooth edge without burrs
Coating 3	Health	Health	Rupture	/

3.3. Corrosion resistance of the coatings

3.3.1. Electrochemical properties of the coatings

The corrosion resistance of the coating was evaluated through electrochemical impedance spectroscopy (EIS) and potentiodynamic polarization curve analysis. Figure 10 shows the fitting curves of impedance and modulus phase angle, the data are shown in Table 8. The impedance spectrum in Figure 10a reveals that the coating sample demonstrates a single time constant, indicating no reactivity between the phenolic resin and the solution. At present, the coating applied on the metal surface effectively obstructed the contact pathway between the corrosive solution and the metal matrix. When characterizing the corrosion resistance through the impedance spectrum, a larger radius of the capacitive arc corresponded to an increased coating resistance. The film resistance R_f of the coating, as shown in Table 8, is measured to be 10^6 Ω·cm^2, significantly surpassing that of the original sample. Upon increasing the coating thickness from 2 μm to 10 μm, the resistance of the coating exhibited a corresponding rise from 1.48 × 10^6 Ω·cm^2 to 5.70×10^6 Ω·cm^2, following the variation observed in the capacitive arc.

The minimum impedance modulus $|Z|_{0.01Hz}$ is widely acknowledged as a crucial parameter in the assessment of material corrosion resistance. The results depicted in Figure 10b demonstrate that the $|Z|_{0.01Hz}$ values for each coating surpass an order of magnitude compared to the original, thereby indicating excellent corrosion resistance properties exhibited by the coatings. The Bode diagram revealed that the coating's modulus exhibits an oblique line trend with respect to frequency, indicating that the coating functions as an isolation layer characterized by high resistance and low capacitance. The electrochemical steps predominantly govern the operation of this system, with each coating's fitting circuit employing the first equivalent circuit diagram depicted in Figure 10a (1) [26]. In contrast to the coating system, a passive film forms on the surface of 304 stainless steel. The corrosion process in the solution is governed not only by electrochemical reactions but also by the diffusion of the corrosive solution within the oxide film. Although the impedance curve of 304 stainless steel did not exhibit a second time constant, this phenomenon may be attributed to the dense passive film that prevents

penetration of the corrosion solution. Therefore, for accurate fitting, it is recommended to employ the second equivalent circuit diagram depicted in Figure 10a (2) [27, 28].

The corrosion rate of the coating can be determined through measurement and fitting of the potentiodynamic polarization curve. The potentiodynamic polarization curve is shown in Figure 10c, and the fitting result is shown in Table 8. The self-corrosion current density exhibited a positive correlation with the corrosion rate. As the coating thickness gradually increased from 0 μm to 10 μm, the self-corrosion current density within the sample decreased from 27.6×10^{-8} A·cm^{-2} to 1.44×10^{-8} A·cm^{-2}, resulting in a reduction of nearly 20 times in the corrosion rate from 31.8×10^{-4} mm·a^{-1} to 1.66×10^{-4} mm·a^{-1}. Changes in these data showed that the thickness increase of the phenolic resin coating had a positive impact on the improvement of the coating corrosion resistance and reduced the corrosion rate when the coating soaked in the corrosion solution.

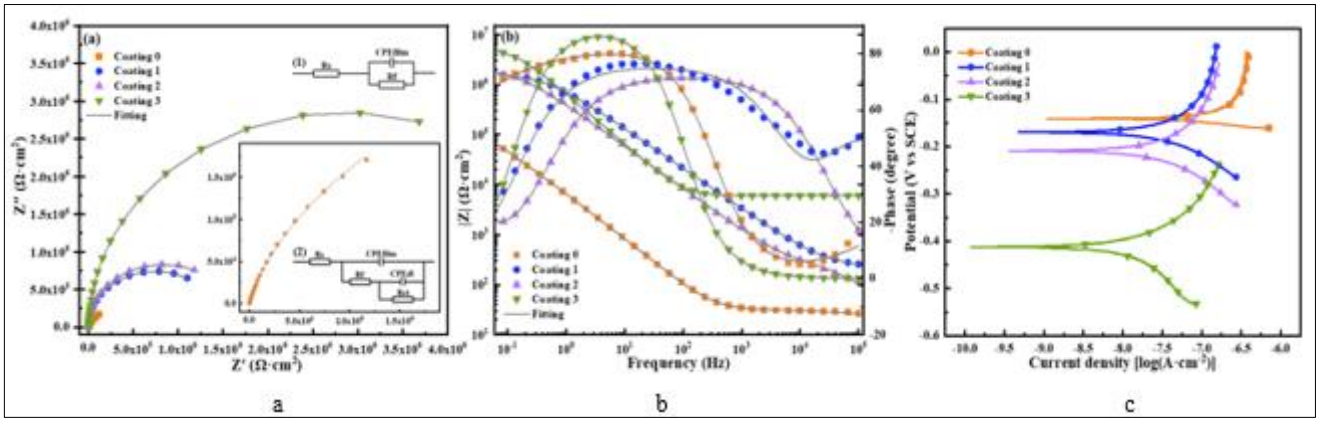

Figure 10. Electrochemical test curves and fitting circuit of each coating:
(a) Nyquist; (b) Bode; (c) Potentiodynamic polarization

Table 8. Electrochemical test curve fitting results of each coating.

Sample	Rs /(Ω·cm^2)	CPE$_{film}$ /(F·cm^2)	R$_f$ /(Ω·cm^2)	|Z|$_{0.01Hz}$ /(Ω·cm^2)	E$_{corr}$ /V	I$_{corr}$/(×10^{-8}A·cm^{-2})	P$_i$/(×10^{-4}mm·a^{-1})
Coating 0	40.3	8.92×10^{-6}	28.51	2.07×10^{5}	-0.140	27.6	31.8
Coating 1	919	9.27×10^{-8}	1.48×10^{6}	1.68×10^{6}	-0.169	10.7	12.4
Coating 2	333	1.80×10^{-7}	1.67×10^{6}	1.88×10^{6}	-0.209	5.43	6.27
Coating 3	6020	2.46×10^{-7}	5.70×10^{6}	4.76×10^{6}	-0.412	1.44	1.66

3.3.2. Long-term service test of coatings

The coating samples were prepared according to GB/T 7901-1999. The corrosion resistance and durability of the phenolic resin coating were further assessed through exposure to wet air hanging specimens and immersion in a 3.5% NaCl solution. In order to ensure the accuracy of measurement, each specimen is individually placed in a beaker, beaker specifications and soaking solution are shown in Figure 11a, b. The distinction between the two hanging experiments lay in the fact that the air hanging experiment evaluated the long-term performance of the coating by quantifying the weight gain and change rate of corrosion products accumulated on the coating samples, while the soaking hanging experiment assessed long-term performance by comparing sample weight loss resulting from dissolution of corrosion products in water. The weight change data per 100 h is presented in Figure 11c, d, e. It can be observed from Figure 11c that the surface of the sample underwent alterations after being exposed to air for 300 h and 500 h, resulting in a significant corrosion area on the surface of the original part. These occurrences can be attributed to defects present in the passive film on the metal surface within this period. The electrolyte solution formed by droplet aggregation and the potential difference between the metal matrix and the passive film constituted the primary battery system, and electrochemical corrosion occurred. The coating samples exhibited only localized pitting corrosion areas, without any significant

signs of extensive corrosion. This phenomenon can be attributed to the presence of tiny surface pores on the coating, as illustrated in Figure 11e.

Smaller droplets permeated through the defects and initiated corrosion on the metal surface. However, owing to the robust interfacial adhesion between the coating and the matrix, diffusion of the corrosive solution was effectively impeded. With the increase in coating thickness, there was a significant reduction in the penetration of defects within the coating, leading to a decrease in the permeation of droplets through the coating and their subsequent contact with the metal matrix. The pitting corrosion was attenuated during this period. In the soaking experiment, as the soaking time increased, Cl^- facilitated the disruption of the passive film on the uncoated metal through adsorption and diffusion. The growth of corrosion products on the metal surface caused the expansion and rupture of the passive film from within, ultimately resulting in severe metal corrosion [29, 30]. The phenolic resin coating exhibited exceptional chemical stability and remained unreactive even in the presence of a 3.5% NaCl solution. The corrosion diffusion inhibition of the coating at this stage was equivalent to that observed in ambient air. However, as the soaking time increased, and the pressure in the water promoted the penetration of the corrosion solution between the metal-coating interface when the corrosion product grew to a certain extent, the coating would be broken off, resulting in the direct contact between the metal matrix and the corrosion solution. Based on the observed corrosion condition of the sample surface, it was evident that an increase in coating thickness led to a reduction in the amount of corrosion products present on the sample surface. Consequently, this enhances the protective performance of the coating on the metal matrix, aligning with the weight change rate depicted in Figure 11.

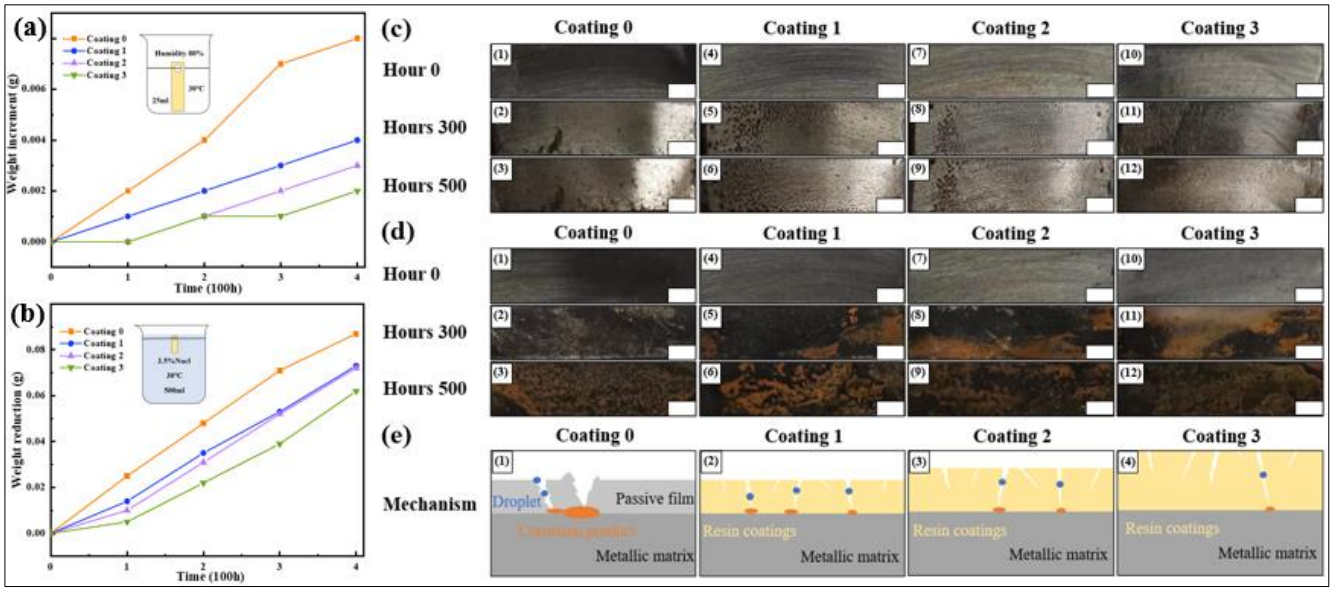

Figure 11. The weight change of each coating for 500 hours: (a) The weight change of wet air hanging specimen; (b) The weight change of the sample soaked in 3.5% NaCl, The surface morphology and corrosion mechanism of each coating after 500h: (c) Wet air hanging specimen; (d) 3.5 % NaCl soaked specimen; (e) Coating corrosion mechanism

4. Conclusions

The phenolic resin coatings exhibit distinct surface roughness variations upon low-temperature curing at 60°C for 24 h while maintaining excellent flexibility and adhesion properties. Remarkably, even after undergoing repeated 180° bending experiments, the coatings remain firmly adhered to the matrix without any signs of damage. The three-dimensional network structure formed by the crosslinking curing reaction between the phenolic resin molecular chains effectively provides a protective barrier for the metal upon impact. The impact resistance of the metal initially increases and subsequently stabilizes with an increase in coating thickness. By investigating the condition of the

coating upon metal fracture, it has been observed that the fracture toughness of the coating exhibits an upward trend with increasing surface roughness. Conversely, coatings with excessively low roughness are prone to brittle fracture when subjected to impact. The coating, with a thickness of roughness of 0.44 μm, exhibits superior comprehensive mechanical properties. It demonstrates excellent adhesion to the metal matrix even after impact, without any observable debris or burrs at the fracture edge.

The application of a phenolic resin coating on the metal surface enhances the corrosion resistance of the metal matrix. The resistance of the sample exhibits a significant increase with an increase in coating thickness, while the capacitive arc radius experiences a tenfold expansion. The self-corrosion current and corrosion rate within the sample decreased by a factor of 19.2 due to an increase in coating thickness. Results from the 500 h wet air hanging test and the 3.5% NaCl solution soaking test demonstrate that both the weight change rate of corrosion products decrease with increasing coating thickness, indicating phenolic resin coating effectively prevents penetration of H_2O and Cl^-, thereby enhancing corrosion resistance and long-term durability of the metal matrix material. This isolation capability exhibits a positive correlation with coating thickness.

Acknowledgments: This work was financially supported by the National Natural Science Foundation of China [Grant Number 51932008, 52074070].

References

1.PAUL, S., Model to Study the Effect of Composition of Seawater on the Corrosion Rate of Mild Steel and Stainless Steel, *J. Mater. Eng. Perform*, **20**, 2011, 325-334. https://doi.org/10.1007/s11665-010-9686-1
2.SHAHEEN, M.A., AFSHAN, S., ATAR, M., Cunningham, L.S., Foster, A.S.J., Experimental testing of stainless steel bolt assemblies at elevated temperatures, *J. Constr. Steel. Res*, **210**, 2023, 108115. https://doi.org/10.1016/j.jcsr.2023.108115
3.KOUBE, K.D., KENNEDY, G., BERTSCH, K., KACHER, J., THOMA, D.J., THADHANI, N.N., Spall damage mechanisms in laser powder bed fabricated stainless steel 316L, *Mater. Sci. Eng. A-Struct. Mater. Prop. Microstruct. Process*, **851**, 2022, 143622. https://doi.org/10.1016/j.msea.2022.143622
4.MILLER, D.M., LILLARD, R.S., An Investigation into the Stages of Alloy 625 Crevice Corrosion in an Ocean Water Environment: Initiation, Propagation and Repassivation in a Remote Crevice Assembly, *J. Electrochem. Soc*, **166**, 2019, C3431-C3442.https://doi.org/10.1149/2.0491911jes
5.DEFORCE, B.S., EDEN, T.J., POTTER, J.K., Cold Spray Al-5% Mg Coatings for the Corrosion Protection of Magnesium Alloys, *J. Therm. Spray. Technol*, **20**, 2011, 1352-1358. https://doi.org/10.1007/s11666-011-9675-4
6.CAI, Q ., LI, S.X., PU, J.B., BAI, X.B., WANG, H.X., CAI, Z.B., WANG, X.Z., Corrosion resistance and antifouling activities of silver-doped CrN coatings deposited by magnetron sputtering, *Surf. Coat. Technol*, **354**, 2018, 194-202. https://doi.org/10.1016/j.surfcoat.2018.09.006
7.MOLLER, V.B., DAM-JOHANSEN, K., FRANKAER, S.M., KIIL, S., Acid-resistant organic coatings for the chemical industry: a review, *J. Coat. Technol. Res*, **14**, 2017, 279-306. https://doi.org/10.1007/s11998-016-9905-2
8.ADHIKARI, A., KARPOORMATH, R., RADHA, S., SINGH, S.K., MUTTHUKANNAN, R., BHARATE, G., VIJAYAN, M., Corrosion resistant hydrophobic coating using modified conducting polyaniline, *High. Perform. Polym*, **30**, 2018, 181-191. https://doi.org/10.1177/0954008316687106
9.BARLETTA, M., PEZZOLA, S., PUOPOLO, M., TAGLIAFERRI, V., VESCO, S., Design, processing and characterization of flexible hybrid coatings: A comparative evaluation, Mater. Des, 54, 2014, 924-933. https://doi.org/10.1016/j.matdes.2013.09.033
10.MATSUZAKI, A., YAMAJI, T., YAMASHITA, M., Development of a new organic composite coating for enhancing corrosion resistance of 55% Al-Zn alloy coated steel sheet, *Surf. Coat. Technol*, **169**, 2003, 655-657. https://doi.org/10.1016/S0257-8972(03)00110-5

11.BAJPAI, P., BAJPAI, M., Development of a high performance hybrid epoxy silicone resin for coatings, *Pigment. Resin. Technol*, **39**, 2010, 96-100. https://doi.org/10.1108/03699421011028680
12.EMIK, S., IYIM, T.B., OZGUMUS, S., Synthesis of silicone-acrylic-modified high-ortho novolac resin with enhanced thermal resistance and surface coating properties, *J. Coat. Technol. Res*, **18**, 2021, 1679-1690. https://doi.org/10.1007/s11998-021-00527-4
13.HERNANDEZ-PADRON, G., ROJAS, F., CASTANO, V., Development and testing of anticorrosive SiO_2/phenolic-formaldehydic resin coatings, *Surf. Coat. Technol*, **201**, 2006, 1207-1214. https://doi.org/10.1016/j.surfcoat.2006.01.070
14. KOTB, Y., CAGNARD, A., HOUSTON, K.R., KHAN, S.A., HSIAO, L.C., VELEV, O.D., What makes epoxy-phenolic coatings on metals ubiquitous: Surface energetics and molecular adhesion characteristics, *J. Colloid. Interf. Sci*, **608**, 2022, 634-643 https://doi.org/10.1016/j.jcis.2021.09.091
15.DEYAB, M.A., DE RICCARDIS, A., BLOISE, E., MELE, G., Novel H2Pc/Epoxy nanocomposites: Electrochemical and mechanical property investigation as anti-corrosive coating, *Prog. Org. Coat*, **119**, 2018, 31-35. https://doi.org/10.1016/j.porgcoat.2018.02.010
16. LIN, Z.M., CHEN, Y.H., MA, Z., GAO, L.H., CHEN, W.H., CHEN, G.H., MA, C., Design and Preparation of Localized Heat-Resistant Coating, *Polym*, 14, 2022, 3032. https://doi.org/10.3390/polym14153032
17.GUO, Y.E., LIANG, P., SHI, Y.H., ZHAO, Y., LI, F., JIN, L., Effect of Hydrogen on Corrosion Behavior of S32750 Super Duplex Stainless Steel, *Int. J. Electrochem. Sci*, 13, 2018, 10302-10313. https://doi.org/10.20964/2018.11.44
18.SUZUKI, S., OGATA, H., UMINO, S., KATO, C., Properties of environmentally harmonized precoated steel sheet for automotive fuel tank use, *Tetsu-To-Hagane*, **89**, 2003, 97-102 https://doi.org/10.2355/tetsutohagane1955.89.1_97
19.LEE, S.J., PYUN, S.I., Assessment of corrosion resistance of surface-coated galvanized steel by analysis of the AC impedance spectra measured on the salt-spray-tested specimen, *J. Solid. State. Electrochem*, **11**, 2008, 829-839 https://doi.org/10.1007/s10008-006-0229-5
20. BIERWAGEN, G., TALLMAN, D., LI, J., HE, L., JEFFCOATE, C., EIS studies of coated metals in accelerated exposure, *Prog. Org. Coat*, **46**, 2003, 149-158 https://doi.org/10.1016/S0300-9440(02)00222-9
21.STEELE, A., BAYER, I., LOTH, E., Adhesion strength and superhydrophobicity of polyurethane/ organoclay nanocomposite coatings, *J. Appl. Polym.* Sci, **125**, 2012, 445-452 https://doi.org/10.1002/app.36312
22.SEONHO, S., HYUNGDAL, P., JINSEOK, K., Characterization and Analysis of Metal Adhesion to Parylene Polymer Substrate Using Scotch Tape Test for Peripheral Neural Probe, *Micromach*, **11**, 2020, 605 https://doi.org/10.3390/mi11060605
23.DUDA, M., PACH, J., LESIUK, G., Influence of Polyurea Composite Coating on Selected Mechanical Properties of AISI 304 Steel, *Mater*, **12**, 2019, 3137 https://doi.org/10.3390/ma12193137
24.LANGER, E., WAŚKIEWICZ, S., KUCZYŃSKA, H., KAMIŃSKA-BACH, G., Self-stratifying coatings based on Schiff base epoxy resins (Article), *J. Coat. Technol. Res*, **11**, 2014, 865-872 https://doi.org/10.1007/s11998-014-9603-x
25.KAR, S., KUMAR, S., BANDYOPADHYAY, P.P., PAUL, S., Grinding of hard and brittle ceramic coatings: Force analysis, *J. Eur. Ceram. Soc*, **40**, 2020, 1453-1461 https://doi.org/10.1016/j.jeurceramsoc.2019.12.058
26.SANTANA, J.J., GONZALEZ, J.E., MORALES, J., GONZALEZ, S., SOUTO, R.M., Evaluation of Ecological Organic Paint Coatings via Electrochemical Impedance Spectroscopy, *Int. J. Electrochem. Sci*, 7, 2012, 6489-6500. https://doi.org/10.1016/S1452-3981(23)19497-1
27.TONG, L.B., ZHANG, J.B., XU, C., WANG, X., SONG, S.Y., JIANG, Z.H., KAMADO, S., CHENG, L.R., ZHANG, H.J., Enhanced corrosion and wear resistances by graphene oxide coating on the surface of Mg-Zn-Ca alloy, *Carbon*, **109**, 2016, 340-351 https://doi.org/10.1016/j.carbon.2016.08.032

28.CHU, J.H., TONG, L.B., WEN, M., JIANG, Z.H., ZOU, D.N., LIU, S.F., ZHANG, H.J., Inhibited corrosion activity of biomimetic graphene-based coating on Mg alloy through a cerium intermediate layer, *Carbon*, **161**, 2020, 577-589 https://doi.org/10.1016/j.carbon.2020.01.086
29.MARTIN, U., RESS, J., BOSCH, J., BASTIDAS, D.M., Stress corrosion cracking mechanism of AISI 316LN stainless steel rebars in chloride contaminated concrete pore solution using the slow strain rate technique, *Electrochim. ACTA*, **335**, 2020, 135565 https://doi.org/10.1016/j.electacta.2019.135565
30.SASAKI, K., BURSTEIN, G.T., Observation of a threshold impact energy required to cause passive film rupture during slurry erosion of stainless steel, *Philos. Mag. Lett*. **80**, 2000, 489-493 https://doi.org/10.1080/09500830050057198

Manuscript received: 29. 08. 2023